Supplementary material

1 - Second harmonic probing from femtosecond pulses

The sample was a 5 mm thick LBO crystal. The 1/e penetration depth of the electric field of the 19 THz pump electric field, convolved with the spectral bandwidth of 5.5 THz FWHM, was 3.2 µm. In order to trace the polarization dynamics in the excited volume, we detected non phase-matched second harmonic generation from 35-fs 800nm probe pulses, generated in a thin layer below the surface.

This second harmonic signal is the homogenous solution to the wave equation, which results from the discontinuity of the optical properties at the boundary of the crystal [27,28]. The generation occurs in a layer below the surface with thickness given by the SH coherence length of $l_c = 1.27\mu m$, over which the dipole emission builds up constructively [27,29,30]:

$$l_c = \frac{\pi}{|k_{2\omega} - 2k_\omega|} = \frac{\lambda}{4|n_{2\omega} - 2n_\omega|}.$$

This SH pulse, which reflects the polarization dynamics in the pumped volume, propagates with a group velocity determined by the linear optical properties and dispersion of the crystal at 2ω.

In addition to this SH signal, a second pulse with wave vector $2k_\omega$ is generated by the fundamental as it propagates through the crystal. This inhomogeneous solution to the wave equation co-propagates both in time and space with the fundamental pulse, therefore with an apparent group velocity determined by the dispersion at ω. Thus, this SH pulse separates both spatially and temporally from the interface-generated SH pulse [28,31] and its intensity is not affected by changes in the excited volume close to the surface (see Figure 1).
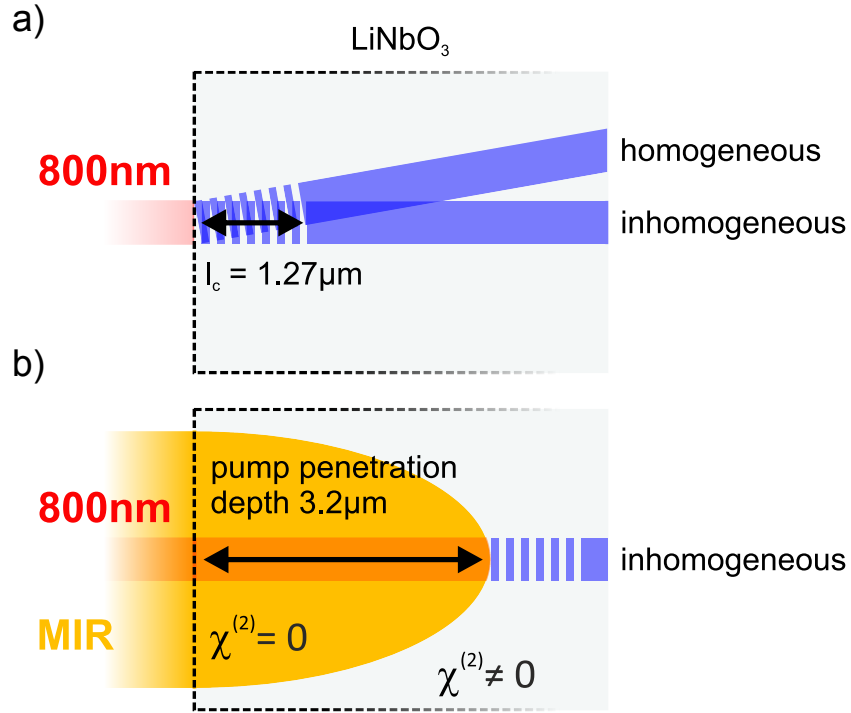
Fig. 1 a) Non phase-matched SH generation in bulk LiNbO$_3$. Two second harmonic signals are generated by the 800nm probe pulses, which separate spatially. The homogeneous solution to the wave equation is generated in a 1.27µm thin layer below the surface. **b)** As the quadratic nonlinearity $\chi^{(2)}$ is depleted within the excited volume, the signal of the homogeneous solution vanishes. In contrast, the SH signal of the inhomogeneous solution is generated in the bulk of the crystal, which is not excited, leaving its intensity unaffected.

These two pulses were separately detected by cross-correlating the total second harmonic radiation emitted from the 5mm thick LiNbO$_3$ crystal, with a synchronized 800-nm pulse in a β-BBO crystal. The measured intensity of the sum frequency is shown in Figure 2 together with a simulation using the SNLO software package (black curve) [32]. The homogeneous solution is delayed by 10.5 ps with respect to the inhomogeneous solution, in good agreement with the simulations. The difference in the relative amplitudes of the homogeneous and inhomogeneous solutions is due to their spatial separation on the detection crystal.

The red curve in Figure 2 shows the same measurement with the sample being excited by the 19 THz MIR pulse at a fixed time delay with respect to the 800 nm pulse. The inhomogeneous solution is almost unaffected due to the limited penetration depth of the MIR pump pulses. In

contrast, the homogeneous solution vanishes due to a complete suppression of the optical nonlinearity χ_2 in the excited volume close to the surface. Hence, changes in the excited surface region can be followed by measuring the SH pulses of the homogeneous solution in transmission through the bulk sample.
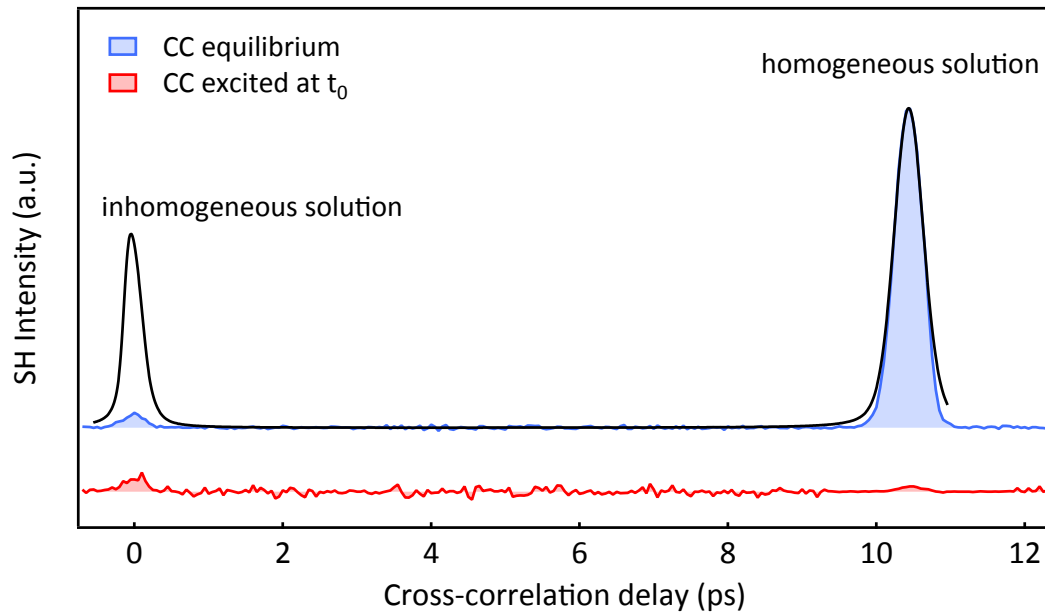

Fig. 2 Cross-correlation between the SH light emitted from the LiNbO$_3$ crystal and a synchronized 800-nm pulse (blue curve). The homogeneous solution to the wave equation, generated at the crystal surface, is delayed by 10.5 ps with respect to the inhomogeneous solution in good agreement with simulations (black line). The excitation of the sample fully suppresses the homogeneous solution while leaving the inhomogeneous unaffected (red curve).

2 - Experimental Setup

Second harmonic intensity measurement

Figure 3 shows the non-collinear pump-probe geometry used in our experiments. An angle of 30° between MIR pump and probe beams was chosen to spatially separate the second harmonic electric fields generated due to quadratic $\chi^{(2)}$ or cubic $\chi^{(3)}$ nonlinearities. The latter process generates a SH field at frequencies $2\omega_{probe} \pm \omega_{MIR}$ by four-wave mixing with the MIR pump pulse, described by the nonlinear polarization

$$P(t) = \varepsilon_0 \chi^{(3)} E_{Probe}^2(t) \cdot \left(E_{MIR}(t) + c.c. \right).$$

As this interaction involves a momentum transfer, the third-order contribution separates spatially from the second-order contribution.
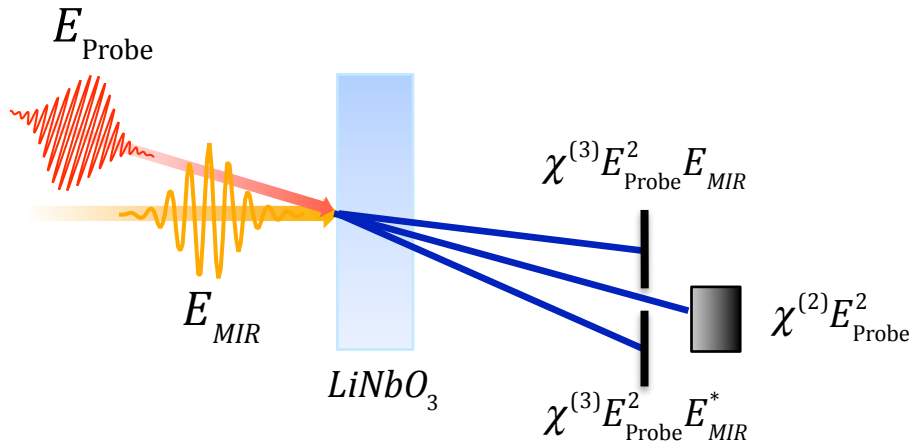

Fig. 3 Sketch of the measurement geometry. The higher order four-wave mixing terms are separated spatially and blocked by a pinhole. The intensity of the remaining second harmonic is then detected with a photomultiplier tube.

Second harmonic phase measurement

The above experimental setup only allows for measuring pump induced changes in the intensity of the SH signal, which holds information on the magnitude of the ferroelectric polarization. To determine the sign of the polarization, we measured the phase of the emitted SH electric field

from the sample at all time delays by interfering it with the SH light generated in a second LiNbO$_3$ crystal. A sketch of the experimental setup is presented in Figure 3a of the main text, showing the measurement of the interference pattern on a CCD-camera. The intensity of an interference fringe at time delay τ between pump and probe pulses is given by

$$I_{SH}(\tau) = \left| E_{SH,\mathrm{Ref}} + E_{SH,0}(\tau)e^{i\varphi(\tau)} \right|^2 = I_{SH,\mathrm{Ref}} + I_{SH}(\tau) + 2E_{SH,\mathrm{Ref}} \cdot E_{SH,0}(\tau)e^{i\varphi(\tau)} + c.c.,$$

where $E_{SH,\mathrm{Ref}}$ denotes the amplitude of the SH electric field from the reference LiNbO$_3$ crystal and $E_{SH,0}(\tau)e^{i\varphi(\tau)}$ the time-delay dependent amplitude and phase of the SH field from the sample. The interference pattern can be extracted by subtracting the contribution from the terms $I_{SH,\mathrm{Ref}} + I_{SH}(\tau)$, which appear as a Gaussian background along the x and y direction of the CCD. A sine-fit to the residual yields $\varphi(\tau)$ as shown in Figure 4.
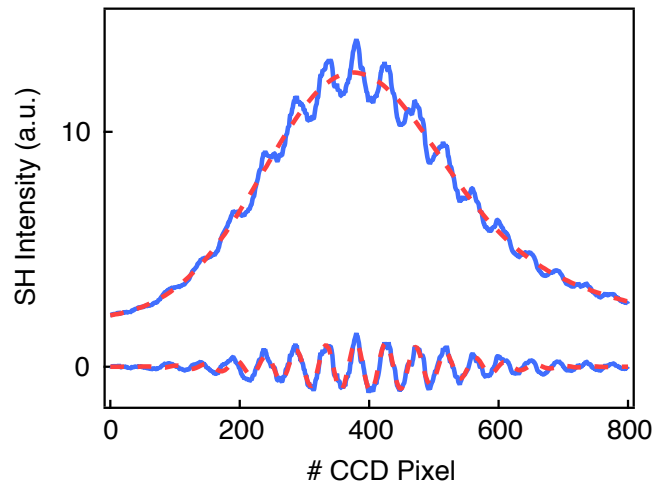

Fig. 4 The time-delay dependent phase of the SH electric field from the sample is obtained by subtracting the Gaussian background from the measured interference pattern and fitting the residual with a sine.

3 - Models of the lattice dynamics

In the following section, we compare the model discussed in the manuscript and an extended model, which takes into account also cubic lattice anharmonicities along Q_P, as calculated in Ref. 11. Considering only the dominant coupling term $aQ_{IR}^2 Q_P$, the response of the crystal lattice to the excitation can be described by the lattice potential energy

$$V = \frac{1}{2}\omega_{IR}^2 Q_{IR}^2 + \frac{1}{2}\omega_P^2 Q_P^2 + \frac{1}{3}b_P Q_P^3 + \frac{1}{4}c_P Q_P^4 - aQ_{IR}^2 Q_P.$$

Here, $\left(\omega_{IR}, Q_{IR}\right)$ and $\left(\omega_P, Q_P\right)$ denote frequencies and normal coordinates of the directly excited and the nonlinearly coupled ferroelectric mode, respectively. The constants b_P and c_P describe the equilibrium lattice anharmonicities.

The left panels of Figure 5 show the potential energy V along Q_P for both the extended model and the minimal model discussed in the main text. At equilibrium, the double well potential exhibits two stable minima, corresponding to the two polarization states ("up" and "down") (Fig. 5(b) black dashed line). The extended model only displays one minimum (Fig. 5(c), black dashed line). In both models, large amplitude oscillations of the driven mode Q_{IR} dynamically induce a new energy minimum with polarization opposite to that of the initial state. Unlike the minimal model without cubic term, the extended model predicts a return of the polarization to the initial value as soon as the coherent oscillations of Q_{IR} decay.

This is also reflected in the dynamical response of the modes to the excitation, which is described by the equations of motion

$$\ddot{Q}_{IR} + \gamma_{IR}\dot{Q}_{IR} + \omega_{IR}^2 Q_{IR} = 2aQ_P Q_{IR} + f(t),$$

$$\ddot{Q}_P + \gamma_P\dot{Q}_P + \omega_P^2 Q_P + b_P Q_P^2 + c_P Q_P^3 = aQ_{IR}^2.$$

A solution to these equations for both the minimal and the extended model is shown in the panels on the right side of Fig. 5. The minimal model predicts permanent polarization reversal as the oscillation amplitude of the mode Q_{IR} exceeds a certain threshold (Fig. 5(b)). For the

extended model polarization reversal is unstable and relaxes back to the initial polarization (Fig. 5(c)). Note that the actual physical situation is not described by either of these models as the coupling to other modes, which is needed to stabilize either polarization state along Q_P are not included explicitly.
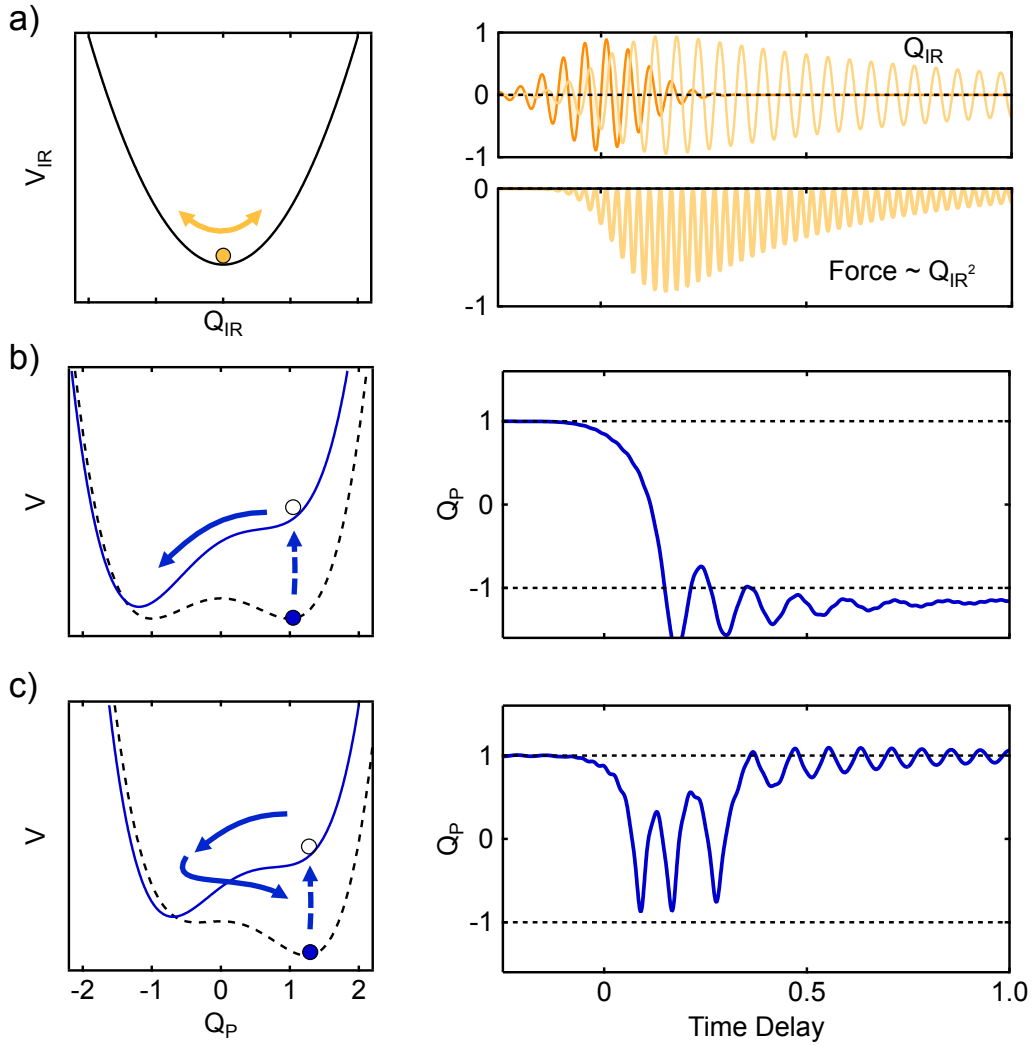

Fig. 5 a) Left: Parabolic energy potential of the resonantly driven infrared-active mode Q_{IR}. Right side: Upon excitation with MIR pulses, the atoms start to oscillate in the potential minimum. As described in the main text, due to the coupling term $aQ_{IR}^2Q_P$ a unidirectional force $\partial V / \partial Q_{IR} = aQ_{IR}^2$ displaces the atoms along Q_P toward the state of opposite polarization. **b)** For the minimal model described in the main text, excitation of Q_{IR} to amplitudes above a certain threshold destabilizes the potential minimum, driving the atoms towards the stable state of opposite polarization. **c)** In case of the extended model, the reversed polarization state is only dynamically stabilized as long as IR-active mode Q_{IR} oscillates at large enough amplitude.

REFERENCES

[27] M. Mlejnek, E. M. Wright, J. V. Moloney, N. Bloembergen, Second Harmonic Generation of Femtosecond Pulses at the Boundary of a Nonlinear Dielectric, *Phys. Rev. Lett*. **83**, 2934 (1999).

[28] V. Roppo, M. Centini, C. Sibilia, M. Bertolotti, D. de Ceglia, M. Scalora, N. Akozbek, M. J. Bloemer, J. W. Haus, O. G. Kosareva, V. P. Kandidov, Role of phase matching in pulsed second-harmonic generation: Walk-off and phase-locked twin pulses in negative-index media, *Phys. Rev. A*. **76**, 033829 (2007).

[29] N. Bloembergen, P. S. Pershan, Light Waves at the Boundary of Nonlinear Media, *Phys. Rev*. **128**, 606 (1962).

[30] P. Schoen, Phase and Polarization Pulse Shaping for Nonlinear Microscopy, *Université Paul Cézanne - Aix-Marseille III*, (2010).

[31] E. Fazio, F. Pettazzi, M. Centini, M. Chauvet, A. Belardini, M. Alonzo, C. Sibilia, M. Bertolotti, M. Scalora, Complete spatial and temporal locking in phase- mismatched second-harmonic generation, *Opt. Exp*. **17**, 3141 (2009).

[32] SNLO nonlinear optics code available from A. V. Smith, AS-Photonics, Albuquerque, NM.